



## NRC Publications Archive Archives des publications du CNRC

### **An Improved Phenomenological Soot Formation Submodel for Three-Dimensional Diesel Engine Simulations : Extension to Agglomeration of Particles into Clusters**

Boulanger, Joan; Neill, W. Stuart; Liu, Fengshan; Smallwood, Gregory J.

This publication could be one of several versions: author's original, accepted manuscript or the publisher's version. / La version de cette publication peut être l'une des suivantes : la version prépublication de l'auteur, la version acceptée du manuscrit ou la version de l'éditeur.

For the publisher's version, please access the DOI link below. / Pour consulter la version de l'éditeur, utilisez le lien DOI ci-dessous.

#### **Publisher's version / Version de l'éditeur:**

<https://doi.org/10.1115/1.2939003>

*Journal of Engineering for Gas Turbines and Power*, 130, 6, pp. 062808-1-062808-6, 2008-11

#### **NRC Publications Record / Notice d'Archives des publications de CNRC:**

<https://nrc-publications.canada.ca/eng/view/object/?id=3fa612e5-048b-4156-bbf4-00ce6b365e46>

<https://publications-cnrc.canada.ca/fra/voir/objet/?id=3fa612e5-048b-4156-bbf4-00ce6b365e46>

Access and use of this website and the material on it are subject to the Terms and Conditions set forth at

<https://nrc-publications.canada.ca/eng/copyright>

READ THESE TERMS AND CONDITIONS CAREFULLY BEFORE USING THIS WEBSITE.

L'accès à ce site Web et l'utilisation de son contenu sont assujettis aux conditions présentées dans le site

<https://publications-cnrc.canada.ca/fra/droits>

LISEZ CES CONDITIONS ATTENTIVEMENT AVANT D'UTILISER CE SITE WEB.

**Questions?** Contact the NRC Publications Archive team at

PublicationsArchive-ArchivesPublications@nrc-cnrc.gc.ca. If you wish to email the authors directly, please see the first page of the publication for their contact information.

**Vous avez des questions?** Nous pouvons vous aider. Pour communiquer directement avec un auteur, consultez la première page de la revue dans laquelle son article a été publié afin de trouver ses coordonnées. Si vous n'arrivez pas à les repérer, communiquez avec nous à PublicationsArchive-ArchivesPublications@nrc-cnrc.gc.ca.



# An Improved Phenomenological Soot Formation Submodel for Three-Dimensional Diesel Engine Simulations: Extension to Agglomeration of Particles into Clusters

**Joan Boulanger**

Gas Turbine Laboratory,  
Institute for Aerospace Research,  
National Research Council Canada,  
1200 Montréal Road,  
Ottawa, ON, K1A 0R6, Canada  
e-mail: joan.boulanger@nrc-cnrc.gc.ca

**W. Stuart Neill**

**Fengshan Liu**

**Gregory J. Smallwood**

Institute for Chemical Process and Environmental  
Technology,  
National Research Council Canada,  
1200 Montréal Road,  
Ottawa, ON, K1A 0R6, Canada

*An extension to a phenomenological submodel for soot formation to include soot agglomeration effects is developed. The improved submodel was incorporated into a commercial computational fluid dynamics code and was used to investigate soot formation in a heavy-duty diesel engine. The results of the numerical simulation show that the soot oxidation process is reduced close to the combustion chamber walls, due to heat loss, such that larger soot particles and clusters are predicted in an annular volume at the end of the combustion cycle. These results are consistent with available in-cylinder experimental data and suggest that the cylinder of a diesel engine must be split into several volumes, each of them with a different role regarding soot formation.*

[DOI: 10.1115/1.2939003]

*Keywords:* soot model, diesel engine, CFD

## Introduction

This short note follows the presentation of a proposed soot model [1] that was essentially developed for engineering purposes, and extends it by introducing agglomeration using the elements exposed in a recent review [2]. This model was originally developed for estimating the soot volume fraction and the primary soot particle diameter. Agglomeration is far from being fully understood. This extension should thus be considered as a somewhat speculative and coarse interpretation of soot particle agglomeration in a cylinder. The qualitative focus may facilitate the comprehension of the in-cylinder pollutant formation process. However, it is important to note that the intent is not to provide comparisons with actual cases and measurements, given our incomplete fundamental knowledge of the processes involved. Rather, it is to assess the behavior and impact on modeling of such refinements and the type of information and scenario that may be accessed such that further experimental validations and practical use can be planned.

$$\frac{d(\rho N)}{dt} = a(\rho n) - b(\rho n)(\rho N) - H(d_{p1} - d_{pz})(\rho(N - N'))^{4/3}(\rho Y_s(N - N')/N)^{2/3} \pi \left( \frac{6}{\rho_s \pi} \right)^{2/3} \bar{v}_r \quad (2)$$

$$\frac{d(\rho Y_s)}{dt} = \bar{v}_r \frac{\pi d_{pi}^2}{4} (\rho N) [\text{fuel}] n_c \bar{M}_c + \rho_s a(\rho n) \frac{\pi d_{pi}^3}{6} - N A_s S_{ox} \quad (3)$$

$$\frac{d(\rho Z_s)}{dt} = \bar{v}_r \frac{\pi d_{pi}^2}{4} \rho (N - N') [\text{fuel}] n_c \bar{M}_c + \rho_s a(\rho n) \frac{\pi d_{pi}^3}{6} \quad (4)$$

$$\frac{d(\rho N_c)}{dt} = H(d_{pz} - d_{p1})(\rho(N - N'))^{4/3}(\rho Y_s(N - N')/N)^{2/3} \times \pi \left( \frac{6}{\rho_s \pi} \right)^{2/3} \bar{v}_r - \bar{v}_r A \sigma_c (\rho N_c) (\rho N_c) \quad (5)$$

## Soot Formation Submodel

The equations below correspond to the extended model (see Ref. [1] for the base line soot and oxidation models):

$$\frac{d(\rho n)}{dt} = a_0 [\text{fuel}] e^{-T_d/T} + f(\rho n) - g(\rho n)(\rho N) - S'_{ox} \quad (1)$$

Contributed by the Internal Combustion Engine Division of ASME for publication in the JOURNAL OF ENGINEERING FOR GAS TURBINES AND POWER. Manuscript received April 30, 2007; final manuscript received February 15, 2008; published online August 22, 2008. Review conducted by Kalyan Annamalai. Paper presented at the 2006 Fall Conference of the ASME Internal Combustion Engine Division (ICEF2006), Sacramento, CA, November 5–8, 2006.

**Table 1 Kinetics in the soot model. For detailed information, see Ref. [1]. For ease, the basic kinetics from Ref. [3] on which this modeling is based is recalled in the caption:**  $\frac{d(\rho N)}{dt} = a(\rho n) - b(\rho n)(\rho N)$  and  $\frac{d(\rho n)}{dt} = a_0 [\text{fuel}] \exp(-T_d/T) + f(\rho n) - g_0(\rho n)(\rho N)$

$T_a$	21,000 K
$a$	$10^5$ (–)
$f$	100 (–)
$g$	$10^{-15}$ m <sup>3</sup>
$b$	$8 \times 10^{-14}$ m <sup>3</sup>
$a_0$	$2.3 \times 10^{-3}$ Hz
$\rho_s$	1900 kg/m <sup>3</sup>
$D_0$	1 nm

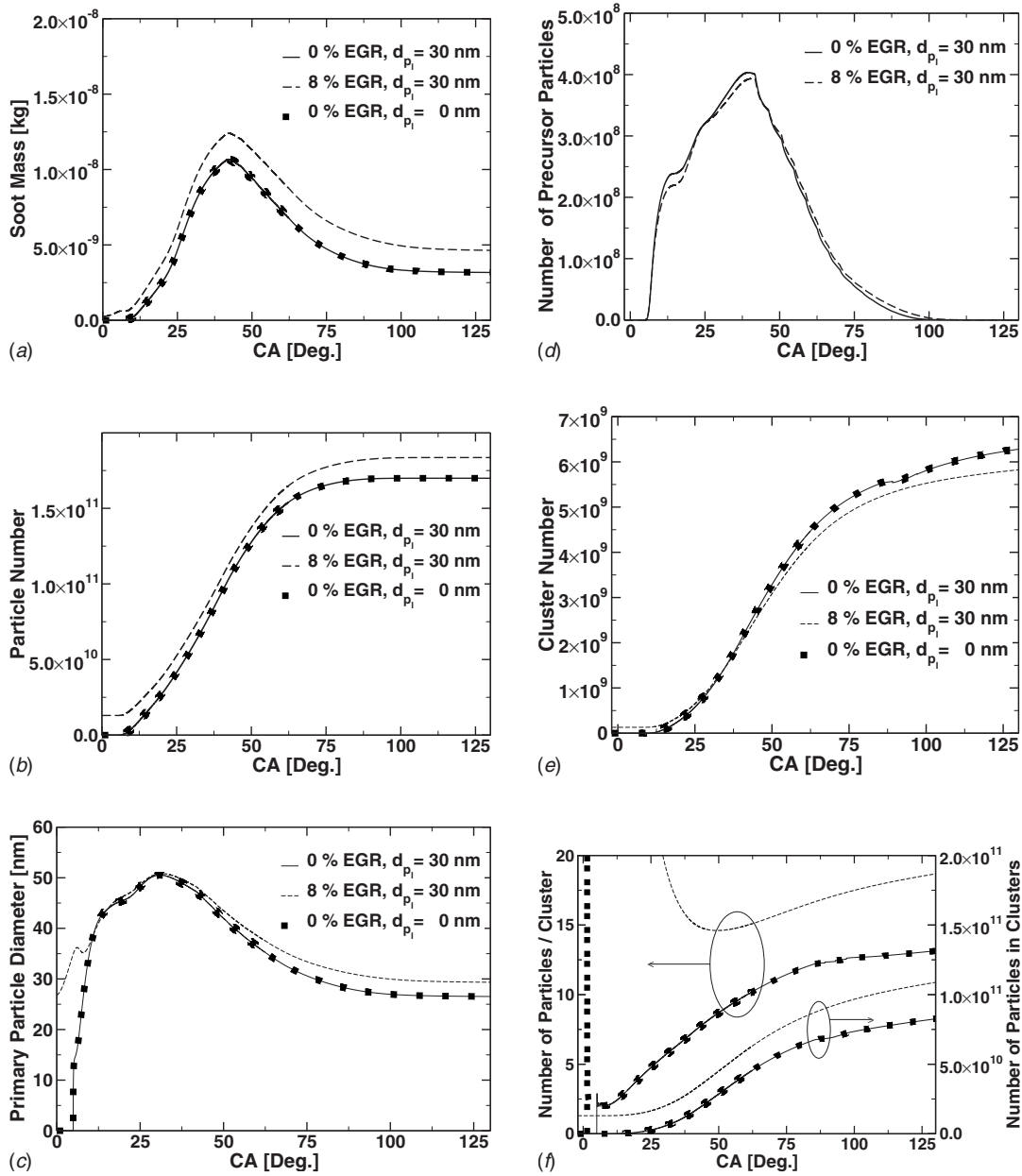


Fig. 1 Soot formation history in the cylinder sector: (a) mass, (b) primary particle number, (c) root mean cubic diameter, (d) precursor particle number, (e) cluster number, and (f) aggregated particles; line: 0% EGR, dashed: 8% EGR, and dots: 0% EGR, no threshold diameter ( $d_{pi}=0$ )

$$\frac{d(\rho N')}{dt} = 2H(d_{pz} - d_{pi})(\rho(N - N'))^{4/3}(\rho Y_s(N - N')/N')^{2/3} \times \pi \left( \frac{6}{\rho_s \pi} \right)^{2/3} \bar{v}_r + \bar{v}_r (d_c/2 + d_{pi}/2)^2 \pi \rho (N - N') (\rho N_c) \quad (6)$$

where  $f$ ,  $g$ ,  $a$ , and  $b$  are the parameters in Ref. [3] for Semenov-type equations;  $T_a$  is the activation temperature of the fuel pyrolysis step;  $\rho_s$  is the density of soot and  $Y_s$  is its mass fraction;  $d_{pi}$  is the inception diameter of soot from radicals;  $a_0$  is the preexponential factor estimating the rate of pyrolysis; [fuel] is the molar concentration of the hydrocarbon (HC) fuel;  $n_c$  is the number of carbon atoms in the HC molecule;  $\bar{M}_c$  is the carbon molar weight; and  $A_s S_{ox}$  and  $S'_{ox}$  are the oxidation terms. Details of these terms are provided in Ref. [1] and their values are quickly recalled in Table 1. The first equation is for the number density of active

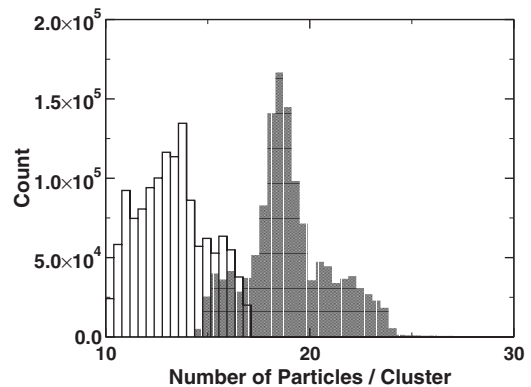
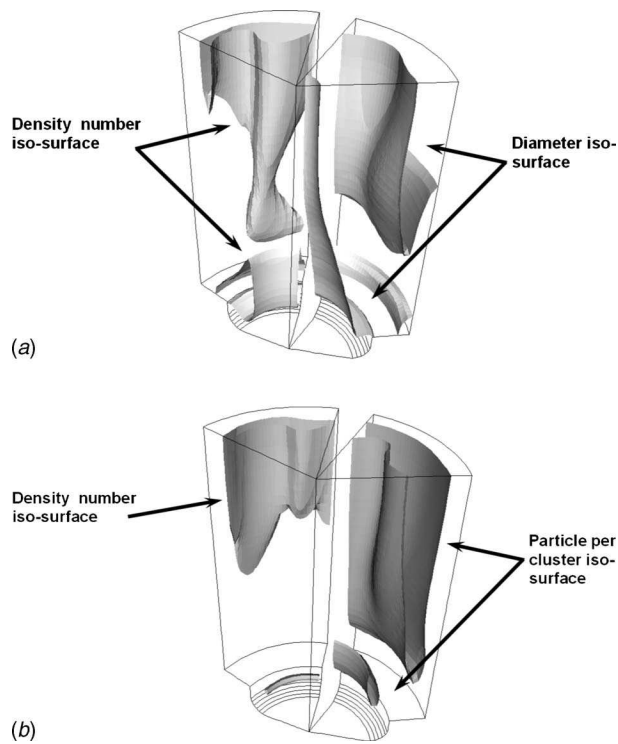
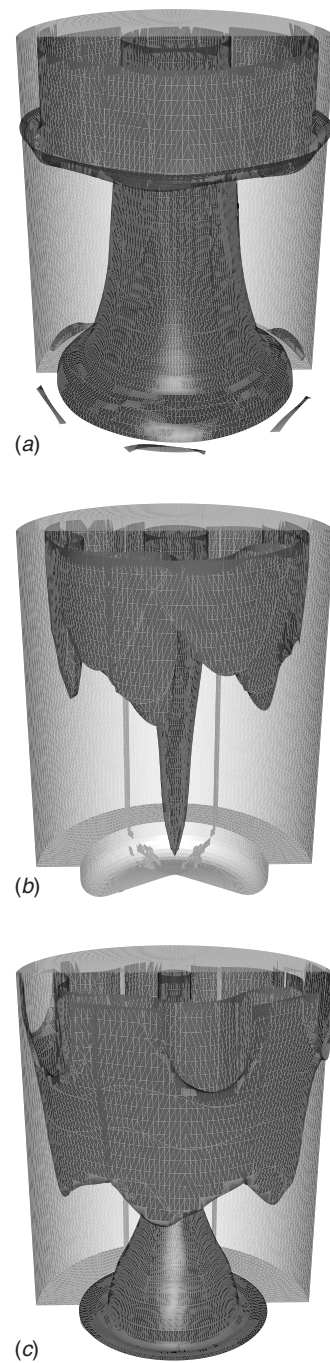


Fig. 2 Distribution of cluster size in terms of particle number; open 0% EGR, and shaded 8% EGR



**Fig. 3** (a) Primary particle location (EVO). Left: density number iso-surface,  $2.3 \times 10^{14} \text{ m}^{-3}$ ; range ( $1.5 \times 10^{13} \text{ m}^{-3}$ ,  $3.3 \times 10^{14} \text{ m}^{-3}$ ). Right: diameter iso-surface. Internal 20 nm. External 30 nm. Range (0 nm, 42 nm), (b) Cluster location (EVO). Left: density number iso-surface,  $1.2 \times 10^{13} \text{ m}^{-3}$ ; range ( $1.5 \times 10^{11} \text{ m}^{-3}$ ,  $1.6 \times 10^{13} \text{ m}^{-3}$ ). Right: particles per cluster iso-surface 14; range (4, 17). Note that the different sectors are the same computational sector representing different quantities.

radicals  $n$  (fuel molecule pyrolysis). The second equation is for the soot primary particle population  $N$ . A third equation based on kinetic theory describes the change in mass  $\rho Y_s$  of the primary particles through growth and coalescence. Evidence is reported in Ref. [4] through transmission electron microscopy (TEM) imaging that agglomeration may happen very early in the cylinder. Hence, new terms extending the model to agglomeration are expressed in the last three equations and the introduction of Heaviside function in the number density equation, Eq. (2). The principle for the present development is the following. A subpopulation  $N'$  of  $N$  particles is considered agglomerating into  $N_c$  clusters. The remaining  $(N - N')$  particles are still free. Each time two free particles collide, they may coalesce (last term of Eq. (2)) or stick and form a structure (first term of Eq. (5)). The transition between coalescence and agglomeration is not obvious [2]. A sensible approach consists in saying that coalescence is no longer possible when the particle is too old, which means that it is solid and the surface is no longer active enough for growth such that it cannot be buried. Size might be a good indication of aging. However, oxidation and coalescence lead to a change in size, which is not related to chemical aging. Thus, a tracer is introduced. This tracer is a virtual soot mass fraction. It is based on free particles and surface growth only (without oxidation or coagulation). This is Eq. (4). When the tracer-particle diameter  $d_{pz}$  is bigger than a threshold diameter  $d_{pf}$ , coalescence is switched off (last term of Eq. (2)) and agglomeration is switched on (first term of Eqs. (5) and (6)). These are the Heaviside functions. Each creation results in two initial particles per structure (first term of Eq. (6)). Structures may collide with free particles (second term of Eq. (6)) and increase their particle number. They may also collide



**Fig. 4** (a) Primary particle diameter field. Internal iso-surface: 17.5 nm. External iso-surface: 35 nm. (b) Cluster size (number of particles) field. Internal iso-surface: 7. External iso-surface: 16. (c) Cluster size (apparent diameter (Ref. [5]),  $d_c$ ) field. Internal iso-surface: 20 nm. External iso-surface: 120 nm.

with each other (second term of Eq. (5)) and form a single bigger cluster.

All collisions are assumed effective. They are based on basic kinetic theory to make the model simple and self-consistent.  $\bar{v}_r$  is the relative velocity between two particles in Brownian motion. Its square is thus equal to the sum of their respective quadratic mean velocities. For modeling, the cluster collision surface, a disk equivalent to the projected surface, is retained. The projected surface, is the sum of the projected surfaces of the primary particles, according to Ref. [5]. This interesting discovery makes the model independent of the fractal parameters, which are acknowledged to

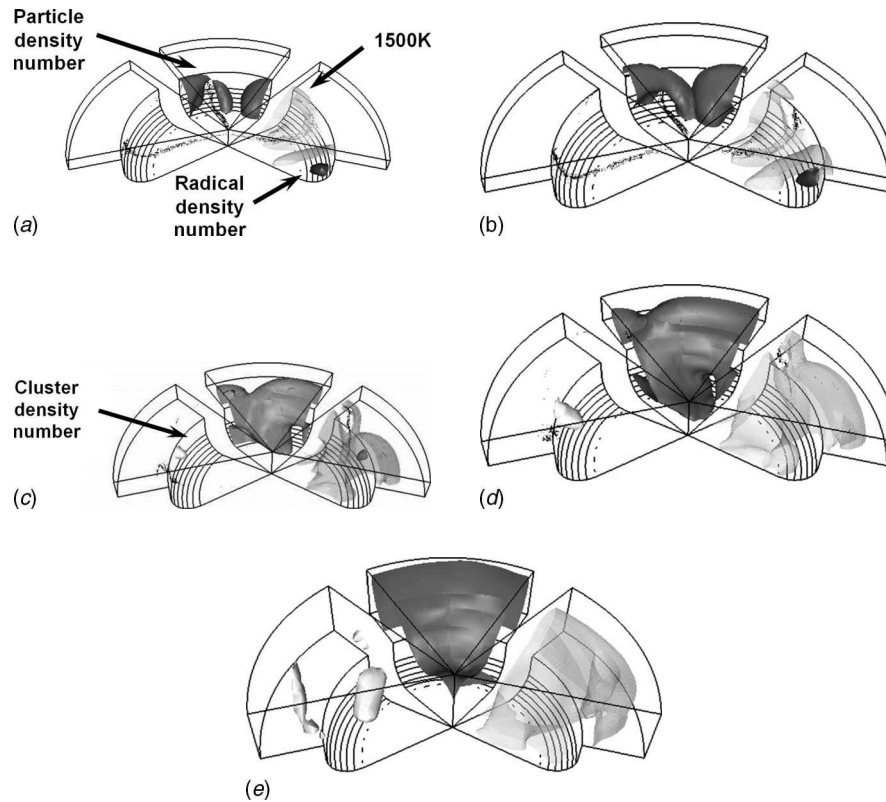


**Fig. 5** Sequence of formation of the soot. Left: cluster density number isosurface,  $1 \times 10^{13} \text{ kg}^{-1}$ . Middle: soot particle density number isosurface,  $1 \times 10^{13} \text{ kg}^{-1}$ . Right: radical density number isosurface,  $1 \times 10^{13} \text{ kg}^{-1}$ . Transparent isotherm at 1500 K. (a) At radical appearance (CA=9.6 ATDC). (b) Close to end of injection (CA =11.7 ATDC). (c) At cluster appearance (CA=18.0 ATDC). (d) At radical disappearance (CA=22.1 ATDC). (e) At full evaporation (CA=34.7 ATDC). Note that the different sectors are the same computational sector representing different quantities.

vary with engine geometry, speed, and load. Thus, the projected surface/collision area is given by  $\sigma_c = \pi d_c^2 / 4 = N' / N_c \pi d_p^2 / 4$ , where  $N' / N_c$  is the number of particles per cluster.  $d_c$  is the estimated diameter of the cluster and  $d_p$  is the diameter of the primary particle. Kinetic theory has limits for complicated structures like fractal aggregates. They may be animated by a complex movement not considered in the theory. Furthermore, their response to turbulent flow may be very different from small soot particles. Aggregation rate may thus be higher than predicted because of a non-representative evaluation of the relative velocity. Empirical approaches have pointed out this problem in typical engine flows [6,7]. This is the reason why comprehensive approaches based on kinetic theory, as in Ref. [8], are of limited utility here. Corrections to augment the Brownian collision rate are very empirical at the present time. It is furthermore hard to believe that they are adapted to the considered configuration. Hence, an arbitrary factor of 100 from the Brownian collision rate appearing in the last term of Eq. (6) has been used to enhance particle clustering in order to maintain simplicity in the model. Tests have demonstrated that change in this factor has marginal impact on soot prediction (except, of course, cluster size) as it has no direct interaction with the soot mass growth. The chosen magnifying factor is arbitrary. Given limited knowledge of this process, it is believed that this qualitative approach is appropriate to highlight phenomena prior to any practical consideration and validation.

The reader is referred to Ref. [1] for the computational framework, tools, and configuration.

## Results and Discussion

An overview of the simulation results is provided in Fig. 1. Numerous observations may be made: (i) cooled exhaust gas recirculation (EGR) increases soot emissions by enhancing both the particle number density and the particle size through a lower overall temperature regarding soot combustion during the expansion stroke and a higher equivalence ratio due to the presence of a vitiated mixture. These are the known prediction capabilities for this kind of model [1]; (ii) pyrolysis of fuel into soot precursors is known to be dependent on both temperature and fuel. This is properly accounted for as the formation of soot precursors is slightly delayed and is smaller for the EGR case. This leads to a time delay before the soot forms in the combustion chamber. The lower temperature in the cylinder for the EGR case slightly reduces the early formation of soot precursors. On the other hand, EGR leads to more soot precursors later in the expansion stroke; and (iii) the choice of a threshold diameter  $d_{p1}$  to turn coagulation into agglomeration is of little importance in the chosen framework. This numerical artifact is due to the Brownian-based coagulation rate being too low, as discussed earlier. In addition to the fact that contemporary knowledge does not allow any solution for this issue, the extremely fast maturation of soot particles proposed (and still debated) in literature [2] may be explained, below.

EGR leads to a slightly smaller number of clusters being formed. This might be due to a reduced early collision frequency between free primary particles. This frequency is dependent on temperature. However, the number of particles per cluster is

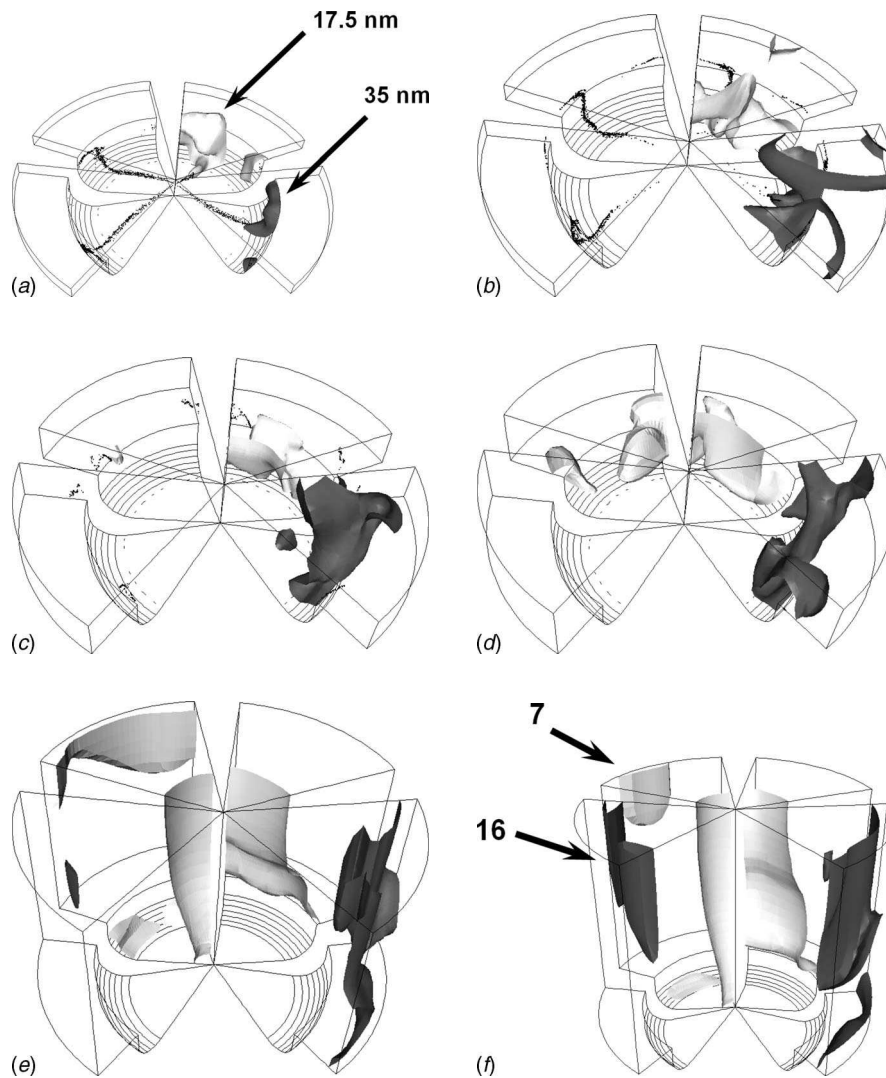


**Fig. 6 Sequence of formation of the soot. From left to right. Particle per cluster isosurface=16. Particle per cluster isosurface=7. Primary particle size isosurface =17.5 nm. Primary particle size isosurface=35 nm. (a) Appearance of particles larger than 45 nm (CA=9.6 ATDC). (b) Close to the end of injection (CA=13.8 ATDC). (c) Appearance of clusters larger than seven particles (CA=26.3 ATDC). (d) End of evaporation (CA=34.7 ATDC). (e) Appearance of clusters larger than 16 particles (CA=72.7 ATDC). (f) CA=93.3 ATDC. Note that the different sectors are the same computational sector representing different quantities.**

larger. The dashed upper curve in Fig. 1(f) for the EGR case predicts that the number of particles in a cluster decreases and then increases. This trend occurs because the soot clusters that are recirculated into the combustion chamber due to cooled EGR are assumed to be fully mature with an average size of 100 particles.

In contrast to the primary particle formation, the threshold diameter  $d_{p_i}$  to switch from coagulation to agglomeration is visible in cluster dynamics. In Fig. 1(f), the start of the cluster formation is revealed by the singularity on the left hand side of the graph. There are a few degrees crank angle between the 0 nm and 30 nm cases. This is negligible. Transition at 0 nm means that the particles are never able to merge. On the other hand, transition at 30 nm involves more mature particles after a long process of surface growth and notable changes of surface chemistry. This is consistent with the fast maturation of the primary particles, as discussed above, showing that the coagulation rate may be of limited importance. It is noted that the existence of soot particles at top dead center (TDC) in this case is simply due to the re-

injection of the soot-containing exhaust gas (without filter) into the intake.

For the following figures, isovalues have been chosen arbitrarily to help the reader interpret the location of the species of interest. Furthermore, when a range of values is present in the caption, it is only for information purposes about the order of magnitude involved. This range is not represented in the picture.

Distribution of the cluster size at exhaust valve opening (EVO) predicted by the numerical simulation is given in Fig. 2. The distribution shape is about the same for the non-EGR and EGR cases. The overall size is thus shifted to EGR as more particles tend to agglomerate.

Figure 3 gives comparative information about soot particles and clusters at the end of the expansion stroke. Consistent with our previous communication [1], bigger particles are found close to the cylinder wall and head. The proposed model is thus able to reproduce the trends experimentally observed [9,10]. It allows one the interpretation that heat loss prevents the oxidation of primary particles. It has actually been shown that emission prediction in

the near-wall region is dramatically impacted by the surface temperature [11]. Oxidation is highly temperature dependent. The number density of particles is more important at the intermediate annular location in the cylinder, an area swept across by spray combustion. In regions close to the wall, where both particle diameter and number density are large, agglomeration is expected to be important. Figure 3(b) displays the presence of numerous agglomerated particles in this region. Both numerous clusters and numerous particles per cluster are found. Like the primary particle distribution, clusters tend to be larger close to the wall. This is consistent with the experiments as well. Growth, coagulation, and agglomeration are acknowledged to be simultaneous. It is thus admitted that some of the largest particles experimentally found may come from a more-or-less buried cluster, i.e., stuck particles are buried by surface growth.

A complete picture of the primary particle location with respect to size is provided in Fig. 4(a). A conical volume around the cylinder axis and embedding the bowl is filled with small particles. A crown of large particles is located close to the corner between the top and the wall. Small particles are explained because of oxidation. The interior of the cylinder volume is a well-mixed high-temperature zone throughout the combustion process. In contrast, the engine cooling system leads to heat losses at the boundaries. They are mainly located at the head and the wall. The oxidation of the soot is thus difficult in these regions. This leads to larger particles. The same formation history is exhibited by clusters, as shown in Figs. 4(b) and 4(c). Small clusters are present along the axis, consistent with the observations made about the results shown in Fig. 3. Numerous large particles have, however, agglomerated in a crown close to the top of the cylinder, according to the mechanism described previously. This provides the picture of particle formation at the end of the expansion stroke and before entering the exhaust pipe. Further agglomeration is expected to occur there.

A history of the soot formation is given in Fig. 5. The iso-1500 K defines a volume where the temperature is higher, as the transition criterion from ignition to combustion. In Fig. 5(a), radicals and soot particles are formed in rich, high-temperature zones. These zones are on the side of the spray and between the spray paths as swirl entrains a rich mixture fed with evaporating fuel. Over time, clouds of soot grow in the proximity of the spray, as shown in Fig. 5(b). Then, clusters begin to appear in the area where the density of soot particle is high, as shown in Fig. 5(c). This area is of an annular shape with a diameter roughly of the order of the bowl. The shape of this area is explained by the presence of evaporating spray, impacting close to the edge of the bowl and mixing with hot air. It is in this rich region where the

soot is formed. During the expansion stroke, this region is simply stretched in the direction of the downward motion of the piston. The result is the field observed in Figs. 3 and 4. Figure 6 displays another picture of the described phenomena. Particles of the soot are formed very early, as exhibited in Fig. 6(a). They easily reach a large size in the rich, high temperature zone in the vicinity of the spray, Fig. 6(b). Clusters appear later and slowly grow, Figs. 6(c)–6(e). As mentioned before, they preferably appear and grow at an annular location that corresponds to a zone where numerous and large particles are found.

## Acknowledgment

This research has been made possible by the funding received from the Government of Canada Program for Energy Research and Development (PERD/AFTER). The authors wish to thank Dr. S. C. Kong and Professor R. D. Reitz for providing the grid specification of the engine geometry and parameters. Dr. William Wallace is gratefully acknowledged for his fruitful comments regarding the improvement of the manuscript.

## References

- [1] Boulanger, J., Liu, F., Neill, W. S., and Smallwood, G. J., 2005, "An Improved Soot Formation Model for 3-D Diesel Engine Simulations," *ASME J. Eng. Gas Turbines Power*, **129**, pp. 877–884.
- [2] Frenklach, M., 2002, "Reaction Mechanism of Soot Formation in Flames," *Phys. Chem. Chem. Phys.*, **4**, pp. 2028–2037.
- [3] Tesner, P., Snegirova, T., and Knorre, V., 1971, "Kinetics of Dispersed Carbon Formation," *Combust. Flame*, **17**, pp. 253–260.
- [4] Su, D. S., Müller, J.-O., Jentoft, R. E., Rothe, D., Jacob, E., and Schlögl, R., 2004, "Fullerene-Like Soot From EUROIV Diesel Engine: Consequences for Catalytic Automotive Pollution Control," *Top. Catal.*, **30/31**, pp. 241–245.
- [5] Brasil, A. M., Farias, T. L., and Carvalho, M. G., 1999, "A Recipe for Image Characterization of Fractal-Like Aggregates," *J. Aerosol Sci.*, **30**, pp. 1379–1389.
- [6] Khan, I. M., Wang, C. H. T., and Langridge, B. E., 1971, "Coagulation and Combustion of Soot Particles in Diesel Engines," *Combust. Flame*, **17**, pp. 408–419.
- [7] Smith, O. I., 1981, "Fundamentals of Soot Formation in Flames With Application to Diesel Engine Particulate Emissions," *Prog. Energy Combust. Sci.*, **7**, pp. 275–291.
- [8] Kazakov, A., and Frenklach, M., 1998, "Dynamic Modeling of Soot Particle Coagulation and Aggregation: Implementation with the Method of Moments and Application to High-Pressure Laminar Premixed Flames," *Combust. Flame*, **114**, pp. 484–501.
- [9] Shahad, H. A. K., 1989, "An Experimental Investigation of Soot Particle Size Inside the Combustion Chamber of a Diesel Engine," *Energy Convers. Manage.*, **29**, pp. 141–149.
- [10] Leipertz, A., and Dankers, S., 2003, "Characterization of Nano-Particles Using Laser-Induced Incandescence," *Part. Part. Syst. Charact.*, **20**, pp. 81–93.
- [11] Wiedenhoefer, J. F., and Reitz, R. D., 2000, "Modeling the Effect of EGR and Multiple Injection Schemes on I.C. Engine Component Temperatures," *Numer. Heat Transfer, Part A*, **37**, pp. 673–694.